High Resolution Whole Head 3D Susceptibility Mapping at 7T: A Comparison of Multi-Orientation and Single Orientation Methods

S. J. Wharton[1], and R. Bowtell[1]
[1]Sir Peter Mansfield Magnetic Resonance Centre, University of Nottingham, Nottingham, United Kingdom

Introduction: Phase images generated using gradient echo techniques at high field strength show excellent contrast related to the variation of magnetic susceptibility across different brain tissues [1] (Fig. 1a&d). Extraction of accurate anatomical information from phase images is however made difficult by the non-local relationship between the field perturbation, which underlies the phase variation, and the associated susceptibility distribution. Several approaches for calculating magnetic susceptibility from magnetic field measurements made using MRI have been proposed based on the deconvolution of field maps [2-5]. However, this deconvolution is an ill-posed problem requiring careful conditioning, for which a number of methods have been developed, including: (i) combination of phase data acquired at multiple orientations [2, 3]; (ii) k-space thresholding of data acquired at a single orientation [3,4]; (iii) incorporation of structural information using corresponding modulus data (Fig.1b&e) acquired at a single orientation [5]. While the multi-orientation method gives excellent results the need for head rotation is a limitation, particularly in studies involving patients. In contrast, the single orientation methods are simple to implement, but can be susceptible to artefacts. Here, we investigate the efficacy of applying the different conditioning strategies to high resolution 3D data acquired at 7T, first to images of a specially created phantom, and then to *in-vivo* data spanning the whole head, and compare the results of each method in regions showing significant susceptibility variation.

Theory: In the Fourier domain the field perturbation, $\Delta B_z(\mathbf{k})$ (= FT{ $\Delta B_z(\mathbf{r})$}) , produced by a susceptibility distribution, $\chi(\mathbf{k})$, that is exposed to a magnetic field, B_0, is given by $\Delta B_z(\mathbf{k}) = B_0\chi(\mathbf{k}) \times (1/3-(k_z/|\mathbf{k}|)^2)$, where the second term on the right is the FT of the dipolar field, which we write as $C(\mathbf{k})$. $\chi(\mathbf{k})$ can then be calculated via the division of $\Delta B_z(\mathbf{k})$ by $C(\mathbf{k})$. However, $C(\mathbf{k})\rightarrow 0$ over the conical surface where $(k_z/|\mathbf{k}|)^2 = 1/3$, meaning that any noise in $\Delta B_z(\mathbf{k})$ is greatly amplified in these 'badly behaved' regions of k-space. In the multi-orientation (MO) approach, the conical surface appears at a different orientation with respect to $\chi(\mathbf{k})$, in the data acquired at each angle to B_0, thus allowing the effect of the badly behaved k-space regions to be averaged out. In the work described here, the data were thresholded to set $\Delta B_z(\mathbf{k})$ values with $C(\mathbf{k}) < \alpha$ to 0 before combination to form the average k-space field. k-space thresholding can also be used to condition data from a single orientation (SO), but in this case care must be taken in choosing a value of α which is a good compromise between preserving contrast and limiting noise amplification [3]. A more sophisticated single orientation approach is to use an iterative conjugate gradient based regularisation (CGR) algorithm, where the noise amplification is controlled by using prior knowledge of $\chi(\mathbf{k})$, such as edge information based on modulus image data. The inversion problem can then be written as $\min_\chi\{\|W\times FT\{C\chi-\Delta B_z/B_0)\}\|_2 + \beta\|W_gG\chi(\mathbf{r})\}\|_2$ [5] , where W is proportional to the inverse of the phase noise which can be estimated from the SNR of the modulus data, β is the regularisation parameter, W_g is the inverse of the gradient of the modulus data (the edge information) (see Fig1c&f) and G is the gradient operator used to extract edge information.

Methods: An agar phantom containing iron-oxide-doped inclusions with known $\Delta\chi$ values, 0.15±0.01ppm in compartment 1 (P1) and 0.075±0.01ppm in compartment 2 (P2), and a healthy subject were scanned using a multi-stack, 3D FLASH protocol TE/TR = 15/150ms, 192x192x86mm^3 FOV, 0.6mm isotropic resolution, acquisition time 6min, SENSE factor of 2, EPI factor 3, on a 7T Philips Achieva scanner, first at a single orientation, and then at four different orientations with the head/phantom tipped forward, back, and to each side, with the angle of rotation being approximately ±10^o degrees in each direction The modulus data were used to co-register the unwrapped phase data. The phase data were then high-pass filtered to remove slowly varying background fields and scaled by $\gamma B_0 TE$ to yield field maps in ppm, before implementation of the various susceptibility calculation methods. For comparison, ROI's were drawn in P1, P2, and the surrounding agar for the phantom data and in the substantia nigra (SN) and globus pallidus (GP) for the *in*-vivo data. These anatomical regions were selected as they showed a large difference in susceptibility relative to the surrounding white matter (WM), attributed to high levels of non-heme iron.

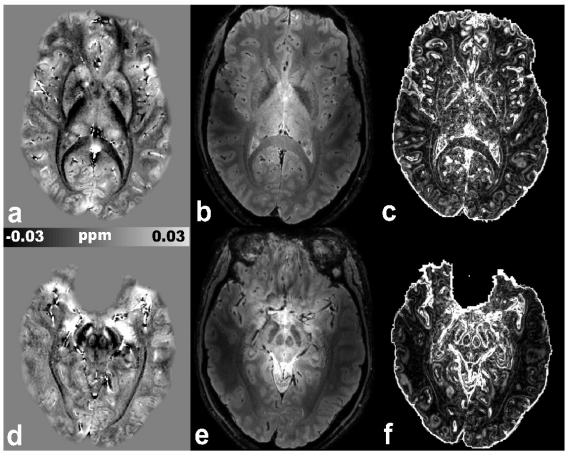

Fig. 1 *Axial slices at the level of the globus pallidus (top) and substantia nigra (bottom), showing filtered phase (a,d), modulus (b,e), and the |gradient| of the modulus data (c,f).*

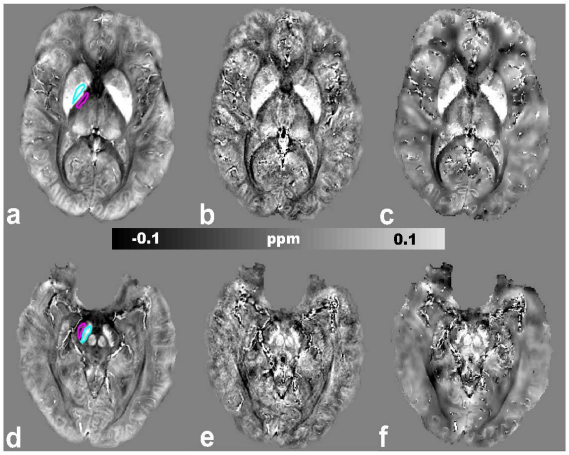

Fig. 2 *Susceptibility Maps calculated using MO method (a,d), SO method (b,e), and CGR method (c,f) ROI's used for Δχ analysis are shown in colour (a,d)*

	MO	SO	CGR
Δχ P1 (ppm)	0.154 ± 0.021	0.134 ± 0.034	0.141 ± 0.029
Δχ P2 (ppm)	0.080 ± 0.023	0.070 ± 0.032	0.078 ± 0.032
Δχ GP (ppm)	0.206 ± 0.019	0.143 ± 0.037	0.158 ± 0.035
Δχ SN (ppm)	0.178 ± 0.041	0.156 ± 0.047	0.174 ± 0.058
ct (min)	5	1	60

Table 1 *Δχ results for phantom compartment 1 (P1) and 2 (P2) relative to surrounding agar, and for GP and SN relative to surrounding white matter, and computation time (ct) for each method for a 64-bit system, 2GHz Dual Core AMD processor.*

Results and Discussion: Optimal threshold values for the MO and SO methods were found to be α = 0.13 and 0.1 respectively, while the CGR method showed good convergence after ~ 50 iterations. The phantom results, detailed in Table 1, indicate that the MO method produced $\Delta\chi$ values in good agreement with expected values, while the SO method underestimated $\Delta\chi$ and produced a larger variation of measured values in each compartment. The CGR method does a better job of preserving contrast and reducing heterogeneity, indicated by the lower error value, compared to the SO method. For the *in-vivo* data the χ-map calculated using the MO method (Fig. 2a&d) showed excellent structural detail with particularly positive susceptibility values in veins and in deep grey matter structures such as the GP and SN (Table 1). The SO method while simple and fast to implement produced maps showing greater heterogeneity compared to the MO method and produced lower $\Delta\chi$ values in the SN and GP. The CGR method yielded higher average $\Delta\chi$-values in the GP and SN compartments compared to the SO method, but still underestimated $\Delta\chi$ values in the GP region compared to the MO data, perhaps suggesting a dependence of the performance of this method on the geometry of the region being analysed. The CGR method required a significantly greater computation time than the other two methods (Table 1). These results indicate that the CGR method offers some advantages for whole-head susceptibility mapping when field data acquired at a single orientation only are available, but that better maps can still be generated by utilising data acquired at multiple orientations. Further work is needed to evaluate whether incorporation of additional a priori information can improve the performance of the CGR method in generating susceptibility maps from single orientation data.

References: **[1]** Duyn et al. 2007. PNAS 104:11796-11801 **[2]** Liu et al. 2009. MRM. 61:196-204 **[3]** Wharton et al. 2009. ISMRM. 463 **[4]** Shmueli et al. ISMRM 2008 p642. **[5]** de Rochefort et al. 2009. ISMRM. 462.